ABSORPTION COEFFICIENT OF CO_2 AND FIRST-ORDER APPROXIMATION OF RADIATIVE FORCING

by

Aleksandar G. Ostrogorsky

Illinois Institute of Technology, IIT, Chicago, IL60616-3793, USA

CO_2 is one of the two primary greenhouse gasses and the source of carbon needed for photosynthesis and life on Earth. The spectral absorption coefficient $\alpha(\lambda)$ [m^{-1}] is a fundamental property of CO_2. It is required for modeling heat transfer at high temperature in furnaces, heat engines, wild fire etc. and in the atmosphere at ~300 K.
Using a FTIR spectrometer, infrared absorbance $A(\lambda)$ spectra of CO_2 were measured with 0.5 cm^{-1} resolution. All measurements were conducted at 295 K. The spectra cover the wavelength range 2 $\mu m<\lambda<18.2$ μm and the pressure range 0.04 atm<p<3atm. The spectra were used to determine the spectral absorption coefficient $\alpha(\lambda)$ in the bands adjacent to the peaks 2.7 μm, 4.26 μm and 15 μm.
The spectra of CO_2 in air are also presented. A first-order approximation-model of the radiative forcing, Δq, is presented. The FTIR spectra confirm that 400 ppm of CO_2 is sufficient to saturate absorption in the central PQR region of the 15 μm band. Consequently, radiative forcing is controlled by the wings (edge) regions of the 15 μm band. 100 % increase in CO_2 concentration will cause radiative forcing, $\Delta q_{400ppm\ to\ 800ppm}$ = 2.79 Wm^{-2}, and temperature increase ΔT ~ 0.7 K. Tenfold (1000 %) increase in CO_2 concentration will increase radiative forcing by ~ 1.8x, so that $\Delta q_{400ppm\ to\ 4000ppm}$ = 5.03 Wm^{-2} and ΔT~ 1.2 K.

Keywords: *Carbon dioxide, absorption coefficient, radiative forcing, transmissivity, greenhouse gases; infrared spectra, climate sensitivity, FTIR;*

1. Introduction

Atmospheric CO_2 is the primary source of carbon needed for photosynthesis and life on Earth. It is one of the two primary greenhouse gasses. Typically,

- CO_2 is released into the atmosphere during combustion of hydrocarbons, breathing, the oceanic carbon cycle, etc.
- CO_2 is removed during photosynthesis while solar radiation is stored as chemical energy – a unique process, only found on Earth.

Photons of visible and infrared (IR) radiation passing through a volume occupied by gas, may be scattered or absorbed by the gas molecules, so that the spectral absorption coefficient $\alpha(\lambda)$ [m^{-1}] is a fundamental property which characterizes the attenuation as a function of wavelengths λ or wavenumbers ν. $\alpha(\lambda)$ [m^{-1}] is needed for heat transfer modeling and computations. Scattering has a minor effect in gasses free of dust or droplets [1-2].

The internal energy of a gas molecule consists of electronic, vibrational, and rotational energy [3]. When IR phonons are absorbed, the vibrational and rotational energy states of the gas are increased. For a gas to absorb IR radiation, there must be a change in the dipole moment of the molecule, so that

- The monoatomic and the symmetric diatomic gases (e.g. N_2, O_2), are transparent to the visible and IR radiation.
- The gases having non-symmetric molecules (e.g. CO_2, H_2O) absorb IR radiation, typically corresponding to wavelength λ ~ 1 to 20 μm, or wavenumbers ν ~ 10,000 to 500 [cm^{-1}][1].

[1] $\nu\left[cm^{-1}\right]=10^4/\lambda\left[\mu m\right]$

Usually, changes in vibrational energy levels are accompanied by changes in rotational energy. Thus, in the absorption spectra, the vibrational lines are surrounded by rotational lines [3]. Furthermore, due to line broadening, the spectral lines are not exactly monochromatic. A bundle of broadened spectral lines forms a band with a maxima at the wavelength specified by quantum mechanics. In the IR region between 2 and 18 μm, CO_2, has three absorption bands with maxima at:

- λ =2.7 μm (3,704 cm^{-1}) caused by a symmetric and asymmetric stretching vibrations.
- λ =4.26 μm (2,347 cm^{-1}), caused by asymmetric stretching vibrations.
- λ =14.99 μm (667 cm^{-1}) due to bending/scissoring.

1.1 IR absorption at high temperature and pressure

Traditionally, the absorbance spectra of CO_2 were needed for modeling thermal radiation fluxes, *q [Wm^{-2}]*, during combustion in furnaces and engines, wild fire etc. As a result, the absorption properties of gases, given in the major heat transfer textbooks, are limited to high temperatures and pressures. For example, the Chapter 14 in Hottel and Sorafim's book [2] is devoted to radiation in flames. The emissivity of H_2O and CO_2 is given by charts developed by Hottel [4] and improved by Leckner [5], where emissivity is wavelength independent, i.e. gray. Therefore, the charts are useful for approximations [6] of radiation heat transfer through gases.

The absorption spectra measured by Edwards [7,8] are given in textbooks by Ozisik [9], Miles [10] and Rohsenow and Choi [11]. The CO_2 spectra were recorded at 1389 K and 10 atm, through a 0.39 m long path [7,8]. Figure 1 a) shows the only absorptivity spectrum of CO_2 given by Siegel and Howell [12], reproduced in Cengel and Ghadjar [13]). As in Edwards, the temperature and pressure of CO_2 are high, 850 K and 10 atm, respectively. Furthermore, all spectra shown in the textbooks are described as low resolution[2].

Figure 1 b) shows the spectral absorptivity of an isothermal mixture of nitrogen and carbon dioxide, given in Modest's book p. 24 [3]. At room temperature (dashed line), the absorption bends are ~2x narrower compared to the bands at high temperature.

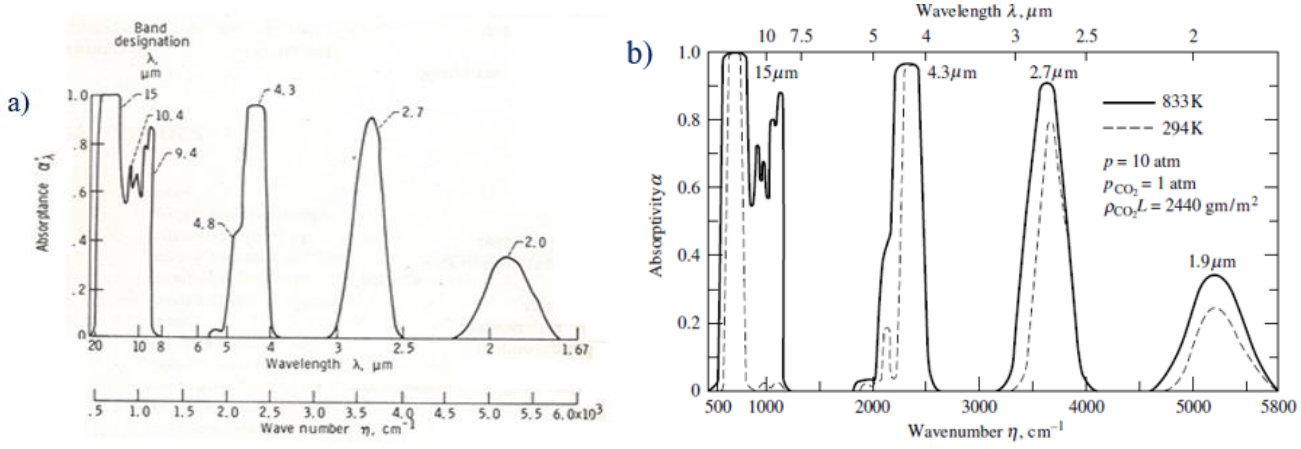

Fig. 1 Absorbance bands of CO2 given in a) Siegel and Howell p.416 [12]. b) Modest, p.24 [3].

[2] Spectral resolution, specified in wavenumbers, cm^{-1}, is ability to distinguish between adjacent absorbance peaks.

1.2 IR absorption at atmospheric pressure and temperature

Heat transfer through the atmosphere is convoluted, including coupled effects of thermal radiation, convection, evaporation, condensation etc. Typically, absorption by CO_2 in the atmosphere can be ignored when distances between the emitting surfaces are in order of a meter. At longer distances, precise computations of radiation heat transfer through air may require accounting for CO_2 and water vapor.

During the past decades, the global warming has emerged as a major issue. Yet, the Modest's book, p.24, may be the only textbook that contains a spectrum of CO_2 relevant to heat transfer in the atmosphere (see dashed line in Fig. 1 b) [3]. This spectrum was reported by Edawards in 1962 [8]. The classic review papers by Howard (1959) [14] and Howard and Garing [15] include the Shaw's spectra [16] of the major greenhouse gases known to occur in the Earth atmosphere, see Fig. 2. Shaw's spectrum is the only CO_2 spectrum given in The Handbook of IR Military Technology (p.228) [17].

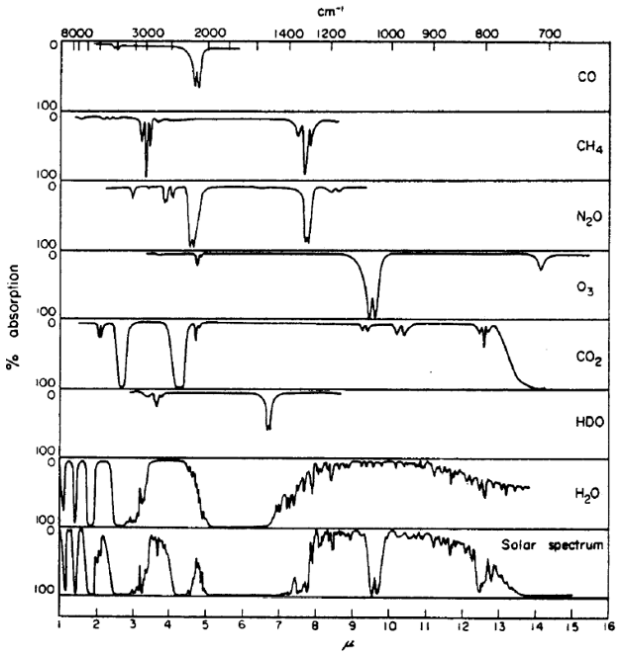

Fig.2 Absorption spectra of "gases known to occur in the atmosphere" [14-17].

Figure 3 a) shows the 1964 spectrum given on the web in the NIST Handbook [18]. The sample is "200 mmHg of CO_2 diluted with N_2". The instrument used is "DOW KBr FOREPRISM" with grating 5.0, 7.5, and 15.0 μm. The development of *Fourier Transfer Infra-Red (FTIR*) spectrometers enabled high spectral resolution measurements. The spectrum in Fig. 3b), was taken using our FTIR spectrometer. Our sample is 156 mmHg of pure CO_2 (see section 3.1). Due to 0.5 cm^{-1} resolution, individual spectral lines were recorded but (in Fig. 3b, plotted to close to distinguish).

In 1973 AFCRL published the first database of individual spectral lines of atmospheric greenhouse gases [19]. The database grew into the HITRAN (*Hi*gh-Resolution *Trans*mission) molecular absorption database. In 2008, it contained more than 2.7 million lines including data for CO_2 and other greenhouse gases [3, 20, 21]. Thus, the advanced models of Earth's climate include line-by-line calculations using millions of data points taken from

the HITRAN database [22,23]. In these models, the term ***Radiative Rorcing (RF)*** is used to specify the difference in the radiation flux, Δq, caused by changes in the concentration of CO_2, other greenhouse gases, clouds, aerosols etc. Yet, the influence of CO_2 on our climate is still controversial in part because the advanced models diverge in predicting the ***Equilibrium Climate Sensitivity (ECS)*** which is a measure for the Earth's temperature increase at doubled CO_2 concentration in the atmosphere. According to the *Intergovernmental Panel on Climate Change (IPCC)*[24], *ECS* is likely to be in the 1.5 C to 4.5 °C range; extremely unlikely less than 1°C, and very unlikely greater than 6°C (see TFE.6, Figure 1, p. 83 in [24]). Yet, according to Harde, "Due to the larger spreads in the solar anomaly and the cloud cover changes we find a maximum range for the ECS of 0.6 °C to 1.2 °C but with a most reasonable value of C_S = 0.7 °C" [22] [3].

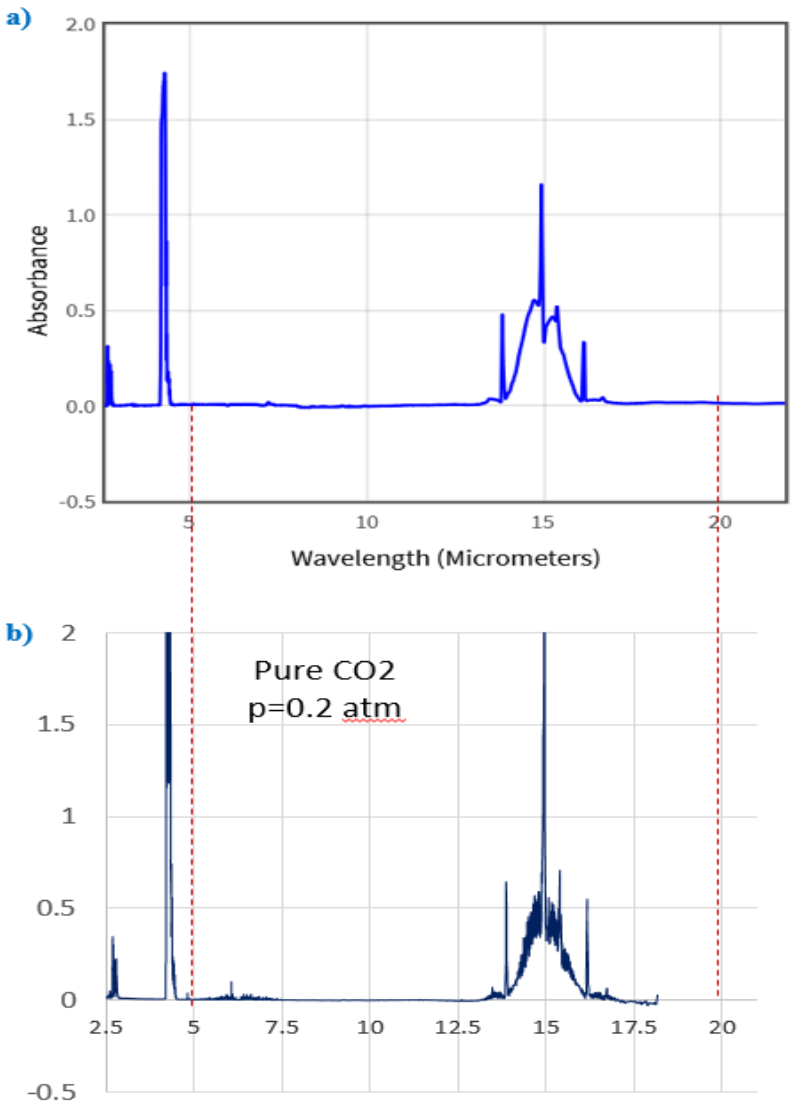

Fig. 3 a) NIST, 200 mmHg of CO_2, diluted in 600 mmHg of N_2. [18]; b) FTIR spectra of pure CO_2, p=156 mmHg.

[3] In [22], C_S denotes climate sensitivity, which is used to specify the increase in Earth's surface temperature ΔT, caused by doubling CO_2 concentration in the atmosphere.

In FTIR spectroscopy, 4 cm^{-1} resolution is recommended for of solid and liquid samples. 2 cm^{-1} is used when be high resolution is required. For spectroscopy of gases, 0.5 cm^{-1} is considered to be sufficiently high to resolve all peaks in a gas spectrum. Thus, our present goal is to:

1) Measure the spectral absorption coefficient $\alpha(\lambda)$ of CO_2 with 0.5 cm^{-1} resolution.
2) Experimentally confirm the *P-Q-R* branches[4] of the 15 μm band are saturated, so that *RF* is caused by increased absorption in the wings region.
3) Present a first-order model of radiative forcing caused by 100 % increase in CO_2 concentration.

2. CO_2 sample confinement and procedure

The measurements were be conducted using the procedure described by Ostrogorsky at al. [25]. The sample compartment of a NICOLET Magna 560 FTIR spectrometer with a KBr beam-splitter and a MCT-A detector[5] cooled by liquid nitrogen, was modified to allow measurement of absorption spectra and the absorption coefficient in gases. A stainless steel conduit with ZnSe windows was placed in the optical path. The conduit was connected to a vacuum system and CO_2 supply (dry ice or a CO_2 tank), allowing operation in the 10^{-5} bar <p< 3 bar range. The ZnSe windows are transparent between 0.5 μm and 20 μm (20,000 cm^{-1} <ν< 500 cm^{-1}).

The *optical transmittance T* of a sample is:

$$T(\lambda) = \frac{I_L(\lambda)}{I_0(\lambda)} \tag{1}$$

where $I_0(\lambda)$ and $I_L(\lambda)$ are respectively, the radiation fluxes entering and exiting the sample. According to the Beer-Lambert Law, the radiation is attenuated exponentially along the path x in the sample,

$$\frac{I_x(\lambda)}{I_0(\lambda)} = \exp\left[-\alpha(\lambda)x\right] \tag{2}$$

The transmittance through a sample is

$$T(\lambda) = \frac{I_L(\lambda)}{I_0(\lambda)} = \exp\left[-\alpha(\lambda)L\right] \tag{3}$$

where *L* [m] is the sample thickness, or the length of the absorption path in the sample. The *optical absorbance A* is,

$$A = \log_{10}\left(\frac{I_0}{I_L}\right) = \log_{10}\left(\frac{1}{T}\right) \tag{4}$$

so that,

$$T = \frac{1}{10^A} \ . \tag{5}$$

[4] In spectroscopy, the *Q*, *P*, and *R* branches correspond to a specific change in the rotational quantum number. When looking at a band, the *Q* branch is in the middle. The *R* branch is at higher frequency (lower λ). The *P* branch is at lower frequency (higher λ).

[5] The recommended range of the MCTA detector with XT-KBr beam splitter and Ever-Glow light source is 11,000 to 600 cm^{-1} (1.35 μm to 16.67 μm).

The intensity of the FTIR modulated beam is attenuated (a) by air outside the vacuum conduit, (b) by absorption and reflection on ZnSe surfaces and (c) by CO_2 in the conduit. The radiation losses are "effective absorbance" accounted for by additive terms,

$$A = A_{CO_2} + A_{air} + A_{ZnSe} \tag{6}$$

Before measurements, the conduit was flushed (evacuated and refilled) three times by pure CO_2. Background absorbance spectra were taken while vacuum (~10^{-2} mmHg ~ 10^{-5} atm) was maintained in the conduit.

$$A_{background} = A_{air} + A_{ZnSe} \tag{7}$$

Subtracting eq. (8) from eq. (7) yields the absorbance along the path of pure CO_2,

$$A_{CO_2} = A - A_{background} = \log_{10}\left(\frac{I_0}{I_L}\right) = 0.4343\alpha L \tag{8}$$

Rearranging yields,

$$\alpha(\lambda) = 2.302\frac{A(\lambda)}{L} \tag{9}$$

For pure CO_2, L=0.19 m. For CO_2 in air, L_{air}=1.9 m [26].

3. Results

All spectra were collected in wavelength range 2 μm < λ < 18.2 μm (5000 cm^{-1} to 550 cm^{-1}).

3.1 Spectral Absorbance A(λ)

In Figure 3, the CO_2 absorbance spectrum given in the NIST Chemistry WebBook [18] is compared to our spectrum. The NIST sample is described as "200 mmHg of CO_2 is diluted with N_2 to a total pressure of 600 mmHg". Our sample is 156 mmHg of pure CO_2. The measured absorbance *A(λ)* of our sample is multiplied by 0.1/0.19, to compensate for the difference in the path length. The bands at 2.7 μm, 4.26 μm and 14.99 μm have identical position and width, demonstrating that 400 mmHg of N_2 did not cause a significant/noticeable broadening of the CO_2 bands. In the NIST spectrum, because of low resolution, the line structure of the band is missing. In contrast, our FTIR spectrum contains N=9,233 points between 2 μm and 18.2 μm (i.e. between 5000 cm^{-1} and 549.6 cm^{-1}). Thus, the individual broadened lines were recorded.

Figure 4 shows the summary of the CO_2 absorbance spectra obtained from dry ice and a CO_2 tank. The three absorption bands are significantly narrower compared to the spectra given in the textbooks, see Fig. 1. Absorbance, A=1, 2 and 3 corresponds respectively to 90 %, 99 % and 99.9 % absorption. Above A=2, the radiation reaching the FTIR detector was weak. For $2<A<3$, the spectra appear to overlap, possibly because the transmitted signal entering the MCT-A detector was at the noise level.

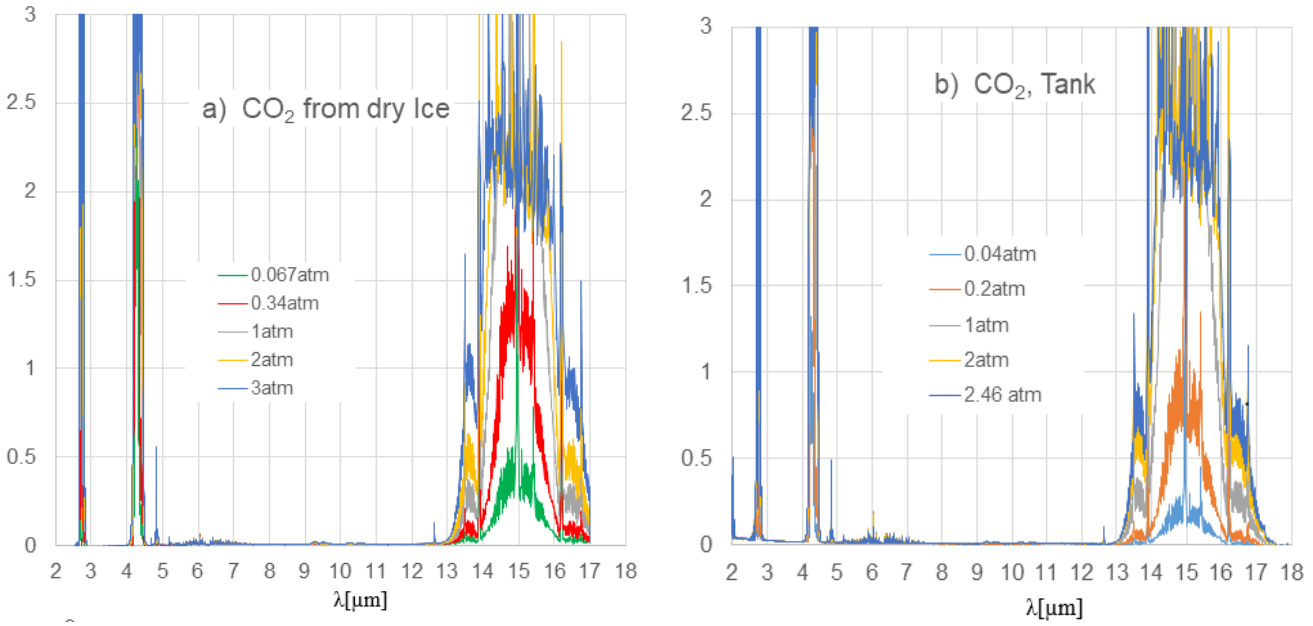

Fig. 4 Spectral absorbance of pure CO_2 at 293 K. Path length L=0.19 m. CO_2 was obtained a) by sublimation of dry ice and b) from a high pressure tank.

In **Figure 5,** the absorption coefficient $\alpha(\lambda)$ is calculated using the measured $A(\lambda)$ and $L=0.19m$ in eq. (9). In the 15 μm band, the Q-, P- and R- branches are evident. The "wings" regions occupy 12.5 μm to 13.8 μm on the R-side and 16.5 μm to 17 μm on the P-side. For clarity, only p≤0.34 atm are shown.

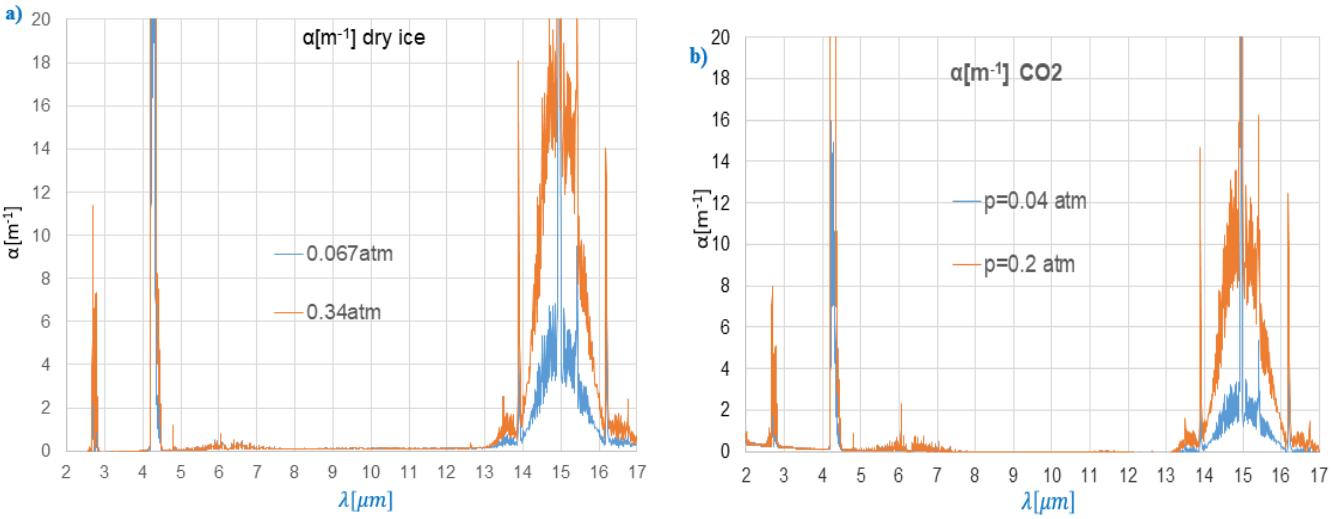

Fig. 5 Spectral absorption coefficient of pure CO_2 at 293 K and $0.04 \le p \le 0.341$ atm. Path length L=0.19 m.

The average value of the absorbance and the absorption coefficient between λ_1 and λ_2 are,

$$A_{\lambda_1 \leftrightarrow \lambda_2} = \frac{1}{N}\sum_{1}^{N} A(\lambda) \tag{10}$$

$$\alpha_{\lambda_1 \leftrightarrow \lambda_2} = 2.302 \frac{A_{\lambda_1 \leftrightarrow \lambda_2}}{L} \tag{11}$$

where N is the number of data points, and $A(\lambda)$ is the absorbance measured at a specific wavelength λ.

3.2-1 The 2.7 μm (3,704 cm^{-1}) band

The absorption coefficient in proximity of the 2.70 μm (ν=3704 cm^{-1}) bend is given in Fig.6. Our FTIR spectra are plotted as a function of ν [cm^{-1}] to facilitate comparison to the spectra given in literature. The spectral absorption coefficient has two bands centered at 3615 cm^{-1} and 3715 cm^{-1}. The number of FTIR data points is N=522, corresponding to resolution Δν/N= 0.5 cm^{-1}.

In Fig. 6 b), Modest and Bharadwaj compare the experiment-based correlations and the data obtained from HITRAN 1996 and EM2C databases. The details related to the data and the correlation lines are given in [27] and p. 374-375 of [3]. Note that the spectra constructed using EM2C database did not capture the dual peaks because of the low resolution, 25 cm^{-1}. The resolution of the HITRAN based spectra is 4 cm^{-1}. At 300 K, the agreement between our spectra in Fig. 6 a) and the data and calculations given in Fig. 6 b) is solid. The bandwidth in Figures 6 a) and b) is equal. Thus, there is no evidence of broadening due to N_2.

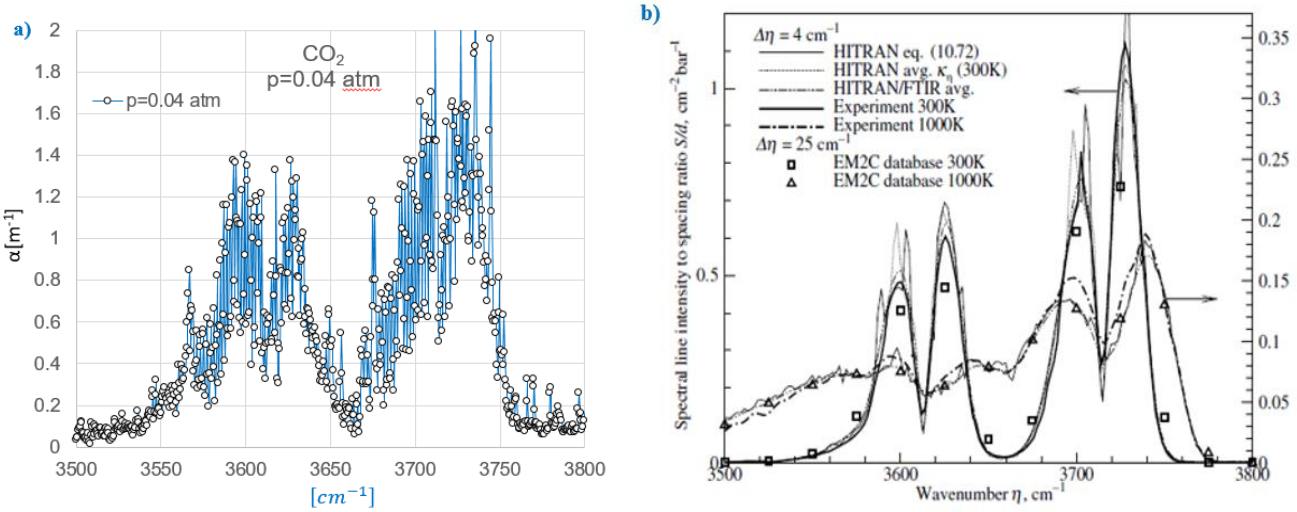

Fig. 6 Absorption coefficient adjacent to the λ=2.70 μm (3704 cm^{-1}) band. a) FTIR spectrum of pure CO_2, 0.5 cm^{-1} resolution. L=0.19 m. b) The 2.7 μm bands of CO_2 at 300 and 1000K are compared with data obtained from HITRAN (4 cm^{-1} resolution) and EM2C (25 cm^{-1} resolution) databases [3].

Figure 7 a) shows the transmittance spectrum, τ(ν), of a CO_2 - N_2 mixture reported by Modest and Bharadwaj [28]. The "pressure" of CO_2 is marked as p= 1 %, 5 % and 50 % next to the corresponding lines in Fig. 7 b). Our spectra shown in Fig. 7 a) correspond to pure CO_2. Additionally, our spectra were taken along a longer path, L=19 cm compared to L=10 cm in [28].

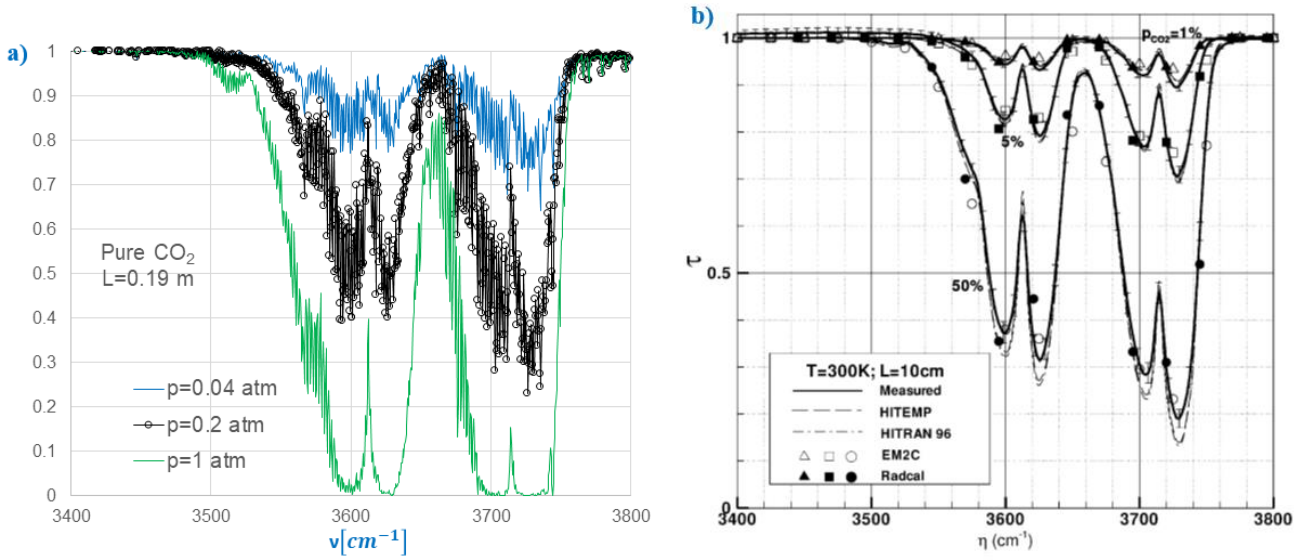

Fig.7 Transmittance in the 2.7 μm band. a) Present spectra, pure CO_2, p= 0.04 atm, 0.2 atm and 1 atm. L=19 cm. b) CO_2 - N_2 mixture [28]. The CO_2 pressure is marked p=1 %, 5 % and 50 % in the figure. L=10 cm.

3.2-2 The 4.26 μm (2,347 cm^{-1}) band

In Figure 8, our spectral absorption coefficient is given as a function of wavenumber $\alpha(v)$, again to facilitate the comparison to the calculated spectrum generated using the HITRAN database given the Modest's book p. 313 [3]. There is no *Q*-branch. The absorption coefficient is remarkably high in the *P*- and *R*- branches. Our FTIR spectrum for pure CO_2 shows a nonzero absorption below 2300 cm^{-1}. Thus, the region between 2250 cm^{-1} and 2285 cm^{-1} may well represent the "wing". The number of data points is N = 332, so that the resolution is $\Delta v/N$= 160 cm^{-1} /332 = 0.5 cm^{-1}. The average value $\alpha_{\lambda_1 \leftrightarrow \lambda_2}$ in the 4.3 μm band is given in Table 1.

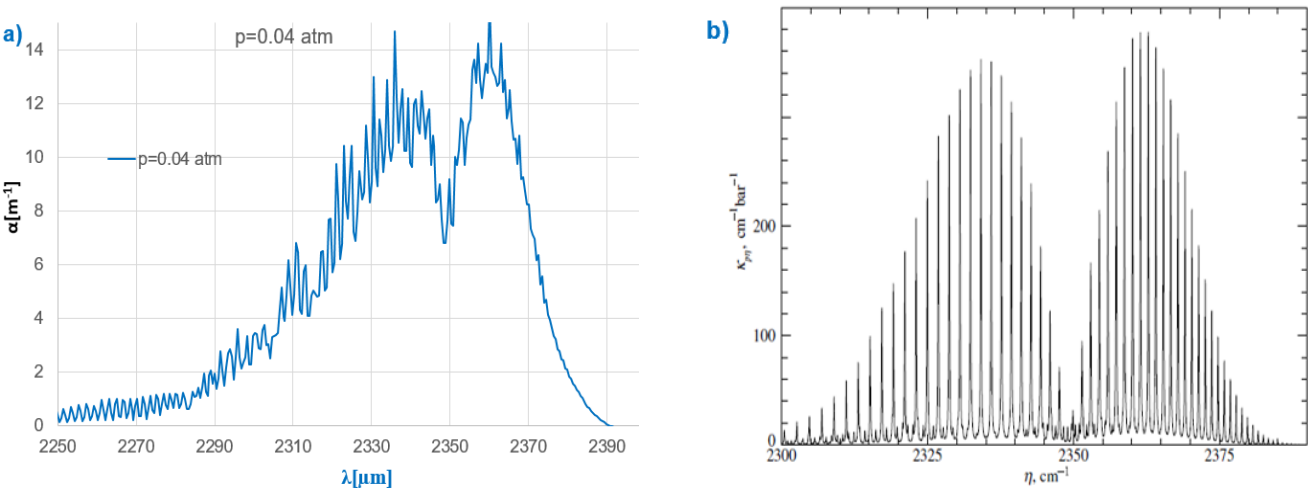

Fig. 8 Absorption coefficient of CO_2 in the λ=4.26 μm (2,347 cm^{-1}) bend. a) Our FTIR spectra for pure CO_2. T=295 K, p=0.04 atm, L=0.19 m. b) Absorption coefficient for small amounts of CO_2 in nitrogen generated from the HITRAN database [3]. p = 1.0 bar, T = 296 K.

3.2-3 The 14.99 μm (667 cm^{-1}) band

Figure 9 shows the absorption coefficient in the 15 μm band due to bending termed "scissoring". For clarity only the spectra taken at p=0.04 atm, 0.2 atm and 1 atm are shown. The central *Q*-branch at 14.99 μm is exceptionally strong. The *R*- and P- branches are located between 13.8 μm and 16.3 μm. In Table 1, the average absorption coefficient in the three bands is compared to the data in [8].

TABLE 1 Absorption coefficients α [m^{-1}] of pure CO_2

		α [m^{-1}]		
Band λ [μm] ν [cm^{-1}].	**Pressure/ mole ratio**	**2.7 μm μm** 2.66 – 2.85 μm 3509-3760 cm^{-1}	**4.3 μm** 4.18-4.48 μm 2232-2392 cm^{-1}	**15 μm** 13-17 μm 588 –769 cm^{-1}
Present data: Pure CO_2. T=295 K L=0.19 m.	1 atm	13.4 11.0	39.9 37.6	14.6 12.6
	0.34 atm	2.96	28.1	5.90
	0.2 atm	2.05	25.4	4.25
	0.067 atm	0.914	11.6	1.948
	0.04 atm	0.594	3.86	1.17
Edwards [8] T=294 K	1 atm, CO_2/N_2 =0.54 mole	1.19	1.28	0.95

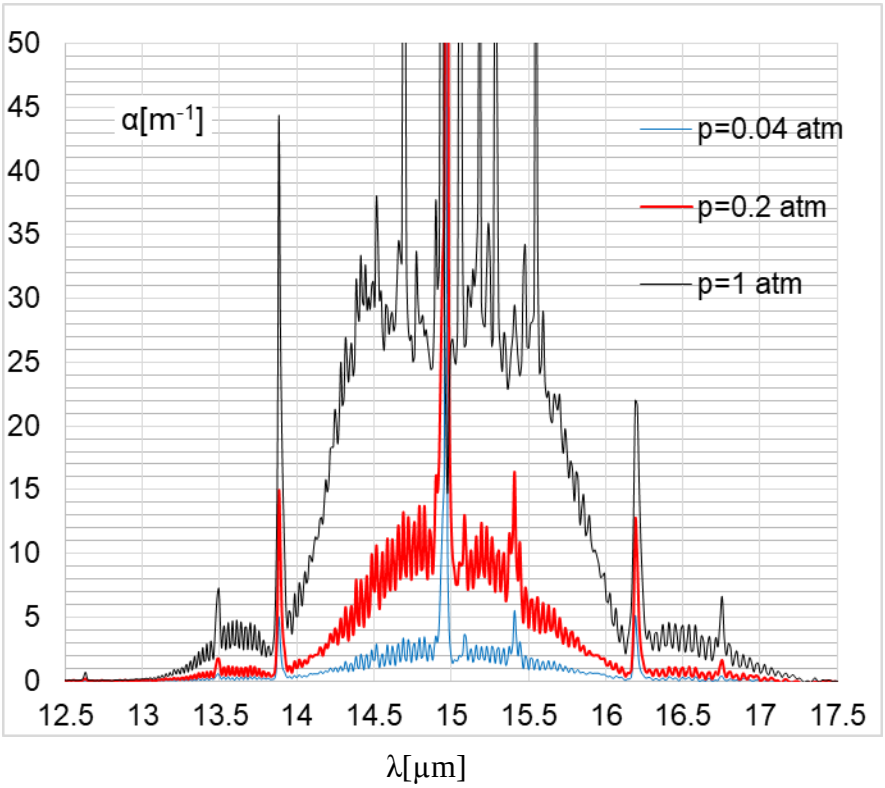

Fig.9 α(λ) of pure CO_2 in the 15 μm band. T=295 K. L=0.19 m.

3.2-4 Absorption in air

Our preliminary spectra are shown in Fig. 10 [26]. The sample is Chicago air, taken with windows wide open in the laboratory. The air temperature was 293 K. The absorption lines of H_2O are located between 4.5 μm and 9 μm and above 16 μm. Using eqs. (10) and (11), the average absorption coefficient of water vapor is $\alpha_{4.5\,\mu m \leftrightarrow 9\,\mu m}$ ~0.15m^{-1}. The fraction of radiation emitted between 4.5 μm and 9 μm is $f_{4.5\mu m \leftrightarrow 9\mu m}$ =0.177.

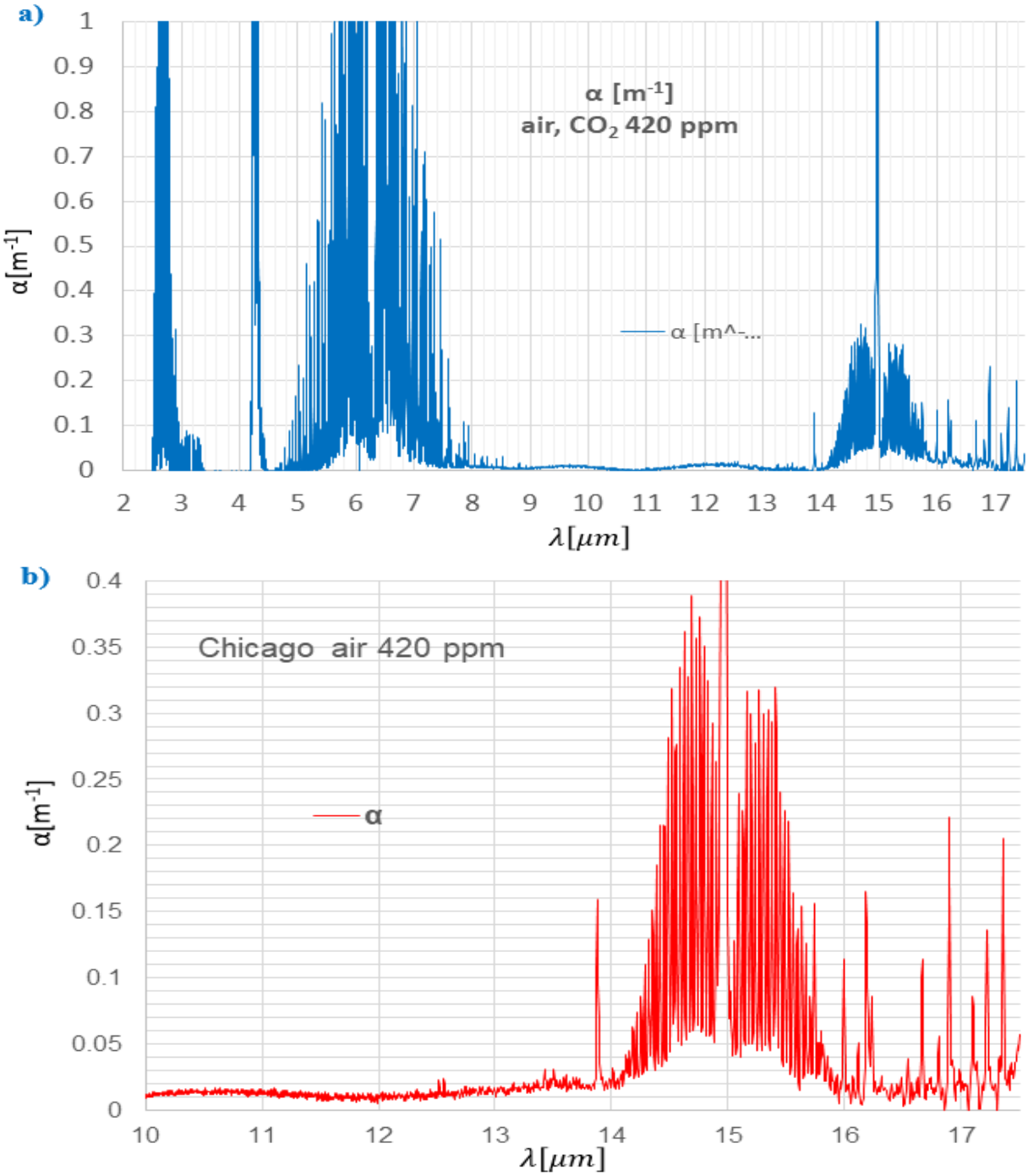

Fig.10 Spectral absorption coefficient α(λ) in air. CO_2 concentration is 400 ppm. a) Three CO_2 bands and absorption lines of water vapor, between 4.5 μm and 9 μm. b) The 15 μm band [26].

In Figure 11, the FTIR spectra given in Fig. 10 are replotted as transmittance, to enable comparison to the spectra reported by Harde [29]. Our spectra in Fig 11 a) were measured along L=1.9 m path. The spectra in Fig. 11 b) were calculated using the HITRAN database, for 380 ppm of CO_2 in dry air and L=1 m. In *P* and *R* branches, our FTIR-measured transmittance is higher than calculated transmittance, although our L is 1.9x higher.

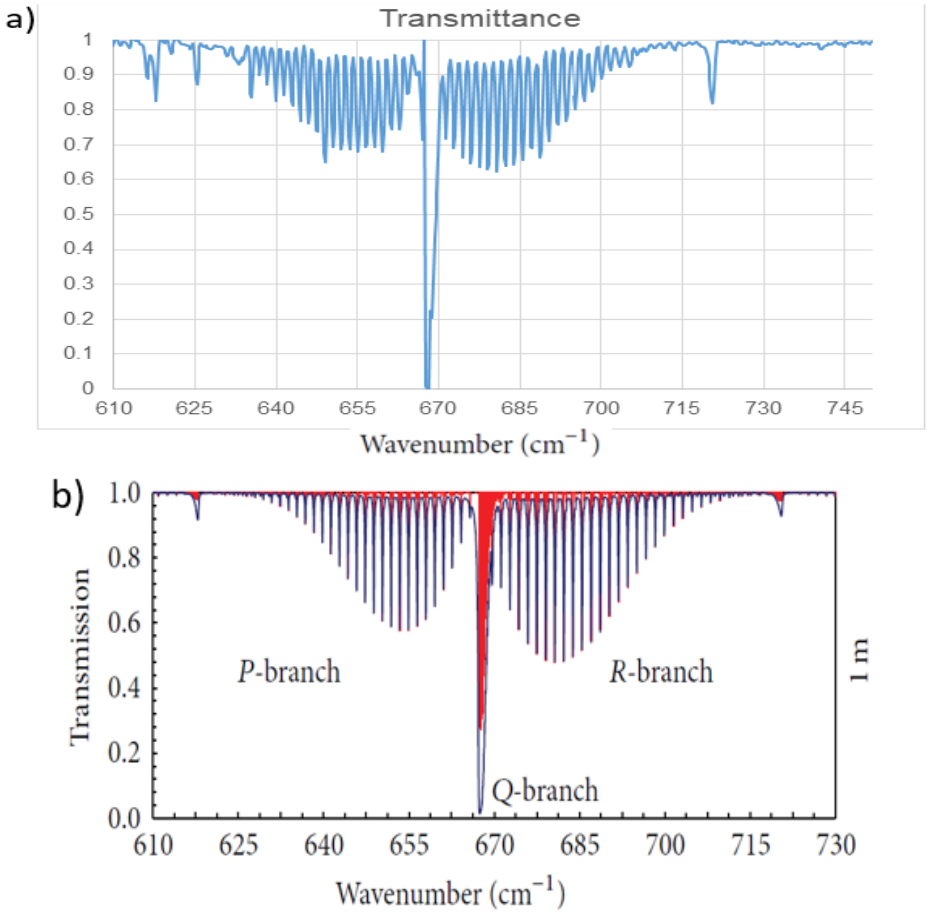

Fig. 11a) FTIR transmittance spectra, Chicago air. L= 1.9 m, T=295. b) Simulated spectra based on HITRAN database, for 380 ppm of CO_2 in dry air, L=1 m, p=1 atm, T=288 K [29].

Table 2 shows the average absorption coefficient in the 15 μm band based on the spectra given in Fig. 10. In the PQR branches, $\boldsymbol{\alpha}$ is close to that used by Wei et al. in [30].

T

TABLE 2 α [m^{-1}] of CO_2 in air at T~293 K.

	α[m^{-1}] 15 μm band		
	P -Q-R branches	**Wings region**	
Range $\lambda_1 - \lambda_2$	**13.8-16.3 μm**	**12.5-13.8 μm**	**16.3-17.5 μm**
$f_{\lambda_1 \leftrightarrow \lambda_2}^{288K}$	0.1167	0.0726	0.0458
FTIR, air, ~420 ppm CO_2	0.085	~0.001	~0.001
400 ppm CO_2 Wei et al. [30]	0.095		

4. Radiative forcing *Δq*

Heat transfer through the troposphere is complex, including convection, evaporation, absorption by greenhouse gases and aerosols, solar irradiance, land use. Thus, the general models considered by the *Intergovernmental Panel on Climate Change, IPCC,* [24,31] include numerous parameters labeled "components" needed to determine precisely the radiative forcing. The general goal is to determine the radiative forcing [Wm^{-2}] and temperature change or climate sensitivity [K] during:

(i) the Industrial Era, from 280 ppm the present day concentration.

(ii) doubling CO_2 concentration, from 400 ppm to 800 ppm.

Fig. 12 shows the radiative forcing (RF) from 1750 to 2011 given in the 2013 IPCC report [31]. Typically, the comprehensive models consider a dozen of components, as listed in Fig. 12. Although models include line-by-line calculations and absorbance spectra stored in the HITRAN database, the uncertainty is high for aerosols, precursors and solar irradiance. In contrast, the uncertainty the CO_2 component is low; the range of RF is from 1.50 to 1.86 Wm^{-2}.

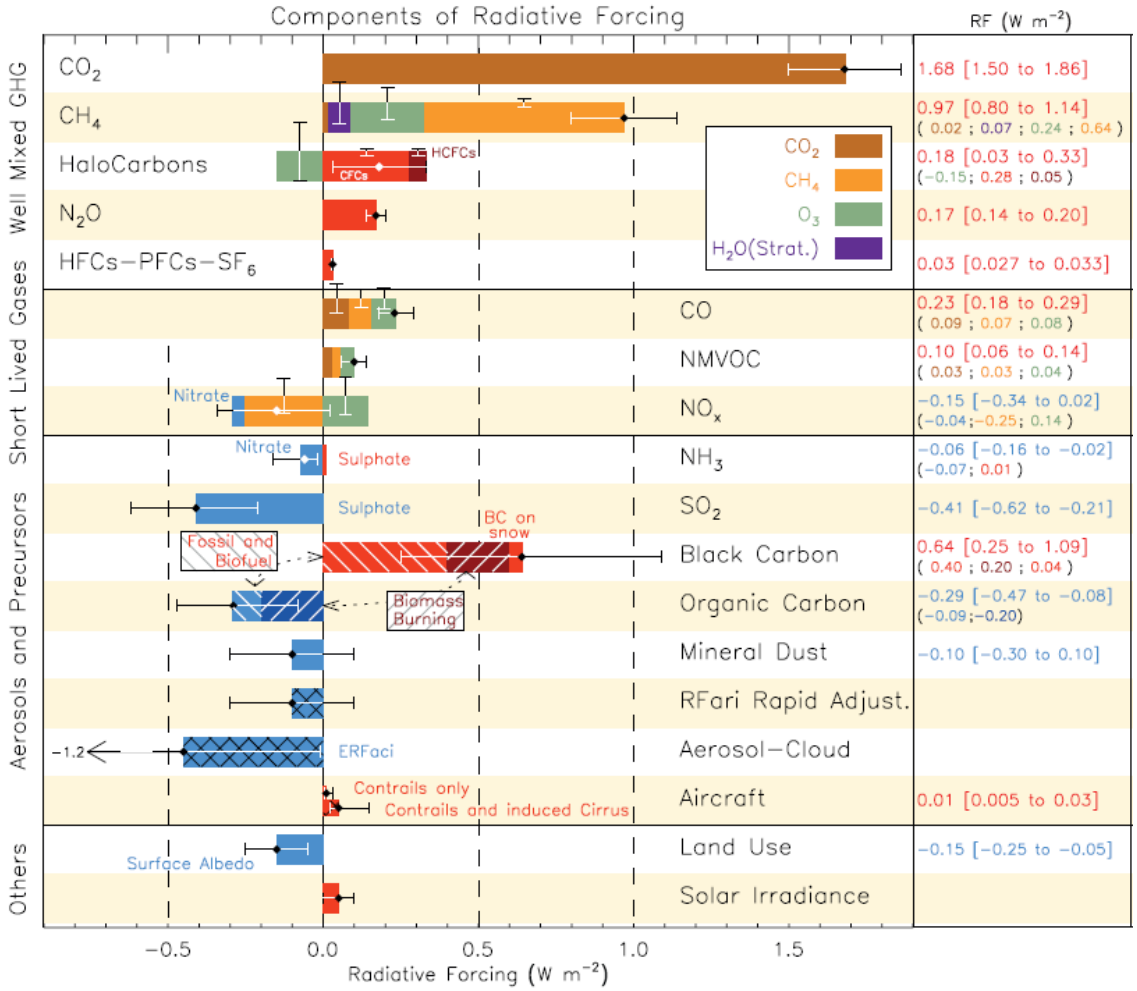

Fig. 12 Radiative forcing (RF) of climate change during the Industrial Era shown by components, from 1750 to 2011. The horizontal bars indicate the overall uncertainty, while the vertical bars are for the individual components. See Fig. TS.7, p.57 in [31] and Fig. SPM.5, p. 14 in [24].

4.1 Direct influence of CO_2 on radiative forcing

Below, the CO_2 spectra in Fig. 10 and 11, are used in a rough approximation considering the first-order effects in radiation heat transfer. The first-order approximations are subject to numerous assumptions and limitations. Yet, a rough "back-of-the-envelope" model may be justified, considering the global advanced comprehensive models "diverge by more than a factor of 10, starting at about 0.4 C and ending at more than 8 C" [22]. Focusing on CO_2 alone, the key assumptions are:

a) No greenhouse gases except CO_2. No clouds or aerosols. The CO_2 concentration is uniform.

b) α=0 between the bands.

c) In the 15 μm band α is proportional to the CO_2 concentration.

d) The Rosseland diffusion approximation is applicable to radiation heat transfer in CO_2[33, 34]

For clarity, below, the subscripts 0, 1,2 and 3 denote:

State 0 Pre-industrial CO_2 concentration, C_0=*280 ppm*.

State 1: The present state, characterized by C_1= *400 ppm*, and T_1 = *288.5 K*.

State 2: A future state, characterized by C_2= *2* C_1 = *800 ppm* (100 % increase)

State 3: A hypothetical state, characterized by C_3= *10* C_1 = *4000 ppm* (tenfold increase)

4.1.1 Emitted radiation

The fraction of radiation emitted by a black surface between λ_2 and λ_1, is equal to,

$$f_{\lambda_1\to\lambda_2}(T)=\frac{\int_{\lambda_1}^{\lambda_2} E_{b,\lambda}\,d\lambda}{\sigma T^4} \tag{12}$$

were

$$E_{b,\lambda}(T,\lambda)=\frac{C_1\lambda^{-5}}{e^{C_2/\lambda T}-1} \tag{13}$$

is the Planks law. T[K] is temperature, C_1= 3.74177153x10^8 [Wm^{-2}] and C_2= 1.4387770 x10^4 [μm K]. Numerical integration of eq. (12) yields the fractions of ***solar radiation,*** emitted at 5,772 K that could be absorbed by CO_2,

$$f_{2.66\mu m\to 2.85\mu m}^{T_{sun}}=4.85\times10^{-3}$$
$$f_{4.18\mu m\to 4.48\mu m}^{T_{sun}}=1.51\times10^{-3}$$
$$f_{12.5\mu m\to 17.5\mu m}^{T_{sun}}=2.4\times10^{-4}$$

Thus, CO_2 has a negligible effect in reducing the incoming solar flux.

The fractions of IR radiation emitted by Earth at 288.5 K, also calculated by precise numerical integration of eq.(12) are given in Table 3, including,

$$f^{T_1}_{2.66\mu m\leftrightarrow 2.85\mu m} \sim 2\times 10^{-5}$$
$$f^{T_1}_{4.18\mu m\leftrightarrow 4.48\mu m} = 1.85\times 10^{-3} \quad (14)$$
$$f^{T_1}_{12.5\mu m\leftrightarrow 17.5\mu m} = 0.235$$

From eq. (14) it is clear that the fraction of thermal radiation emitted by Earth in the *2.7 μm* and *4.3 μm* bands is negligible. Yet, the fraction emitted in the 15 μm band (12.5μm<λ<17.5μm) is 23.5 %. The remaining 76.5 % of IR radiation is emitted by Earth is transmitted through the "windows" with no interference from CO_2 molecules (*Table 3*).

The total flux of thermal radiation emitted by the Earth surface is

$$q^{emitted} = \varepsilon\sigma T^4 \quad (15)$$

where $\sigma=5.67x10^{-8}\ Wm^{-2}/T^{-4}$ is the Stefan-Boltzmann constant. Assuming black body emissivity $\varepsilon = 1$, the total flux of thermal radiation emitted by Earth surface is:

$$q^{emitted\,T_1} = \sigma 288.5^{\ 4} = 392.8\frac{W}{m^2} \quad (16)$$

The flux emitted in the 15 μm band is,

$$q_1^{emitted,\ 15\mu m\,band} = f_{12.5\mu m\leftrightarrow 17.5\mu m}\sigma T_1^4 = 0.235\times\sigma\times 288.5^4 = 92.3\frac{W}{m^2} \quad (17)$$

This flux is split between the *PQR* and the wings region as,

$$q_1^{emitted,\ PQR} = f_{13.8\mu m\leftrightarrow 16.3\mu m}\sigma T_1^4 = 0.1166\times\sigma\times 288.5^4 = 45.8\frac{W}{m^2} \quad (18)$$

$$q_1^{emitted,\ Wing} = \left(f_{12.5\leftrightarrow 13.8\mu m 16.3\mu m} + f_{16.3\mu m\leftrightarrow 17.5\mu m}\right)\sigma T_1^4 = \left(0.0726+0.0458\right)\times\sigma\times 288.5^4 = 46.5\frac{W}{m^2} \quad (19)$$

The flux emitted in the "window" regions (outside of the 15 μm band) is fully transmitted,

$$q_1^{windows} = \left(f^{transparent}_{<12.5\mu m} + f_{>17.5\mu m}{}^{transparent}\right)q^{emitted\ T_1} = \left(0.405+0.3595\right)\times\sigma\times 288.5^4 = 300.3\frac{W}{m^2} \quad (20)$$

The above flux is higher than the actual, because our model assumes that no other greenhouse gases are present.

4.1.2 The Rosseland equation

The Rosseland diffusion approximation is valid in a medium which is optically thick, $\alpha L >> 1$, over the entire spectrum [3,6]. The vertical path in the troposphere is ~ 10^4 *m*. Using the average absorption coefficient in the 15 μm band, αL>> 1, so that we proceed to calculate the Rosseland's "radiative conductivity",

$$k(\lambda)^{radiative} = k_{air} + \frac{16}{3\alpha(\lambda)}\sigma T^3 \ . \quad (21)$$

and radiative heat flux,

$$q(\lambda)^{Rosseland} = k^{radiative}\frac{dT}{dz} = \frac{16}{3\alpha(\lambda)}\sigma T^3\frac{dT}{dz} \quad (22)$$

although CO_2 is transparent between the bands.

TABLE 3. Black body emitted radiation: fractions and flux at 288 K

Band name	λ range	Fraction $f_{\lambda 2 \leftrightarrow \lambda 1}$	Flux $q_{emitted}$ Wm^{-2}
2.70 μm	2.66 μm ↔2.85 μm	$1.573x10^{-5}$	6.12e-3
4.26 μm	4.18 μm↔4.48 μm	0.001854	0.728
15 mμ	12.5 μm↔17.5 μm	0.2350	92.36
PQR branches of 15 μm band	13.8 μm↔16.3 μm	0.1166	45.84
R-wing of 15 μm band	12.5 μm ↔ 13.8 μm	0.0726	28.52
P-wing of 15 μm band	16.3 μm ↔ 17.5 μm	0.0458	17.99
Transparent "window 1"	0 μm ↔ 12.5 μm	0.405	159.1
Transparent "window 2"	17.5 μm ↔ ?	0.3595	141.3

4.2 The Wings Model

According to Harde [29]: "On the *Q*-branch (band center), radiation is almost completely absorbed after a length of only 1m, and with increasing propagation distance, even the weaker lines of the *P*- and *R*-branches reflect totally saturated absorption. At 1 km or more, only the far wings of the band structure still show some rest transmission." The conclusion "totally saturated absorption" fully concurs with our spectra in Fig. 10, where, in the PQR branches $\alpha \geq \sim 0.1$ m^{-1}. The transmission in the central PQR region is negligible. We proceed assuming that:

- The PQR region is opaque.
- Only the wings region participates in radiative forcing.

4.2.1 Radiative forcing from C_0 =280 ppm, to C_1 =400 ppm

According to Fig. 10 b) the range of the wings is 12.5 μm to 13.8 μm on the *R*-side and 16.3 μm to 17.5 μm on the *P*-side. The average absorption coefficient in the wings region is $\alpha_1 \sim 0.001$ m^{-1} for the wings. Using this average value gives for the *State 1*,

$$k_1^{wings} = \frac{16\sigma}{3\,\alpha_1} T_1^3 = 7,261 \frac{W}{m\,K} \ . \tag{23}$$

$$q_1^{wings} \sim \left(f_{12.5 \leftrightarrow 13.8 \mu m 16.3 \mu m} + f_{16.3 \mu m \leftrightarrow 17.5 \mu m} \right) k_1^{wings} \frac{dT_1}{dz} = 0.1184 \cdot 7,261 \frac{W}{m\,K} 0.0065 \frac{K}{m} = 5.59 \frac{W}{m^2} \tag{24}$$

where dT/dz = 0.0065 K/m and $k_{air} \sim 0.025$ $Wm^{-1}K^{-1}$ is ignored. Thus, at present only ~12% of radiation emitted

in the wings is transmitted. In *State 0*, assuming that α is proportional to the concentration of CO_2,

$$\alpha_0 \propto \alpha_1 \frac{C_0}{C_1} = \alpha_1 \frac{280\ ppm}{400\ ppm} = 0.7\alpha_1 \tag{25}$$

so that,

$$k_0^{wings} \propto \frac{16\sigma}{3\left(0.7\alpha_1\right)} T_1^3 = 10{,}373 \frac{W}{m\ K}$$

$$q_0^{wings} \sim f^{wings} k_0^{wings} \frac{dT_1}{dz} = 7.98 \frac{W}{m^2}.$$

Note that $q_0^{wings} = 1.363\, q_1^{wings}$. Radiative forcing due to CO_2, from pre-industrial State 0 to the present State 1is:

$$\Delta q_{0-1}^{wings} = q_0^{wings} - q_1^{wings} = 2.40 \frac{W}{m^2} \tag{26}$$

4.2.2. Radiative forcing from C_1=400 ppm to C_2=800 ppm

Assuming again that α is proportional to the concentration of CO_2 molecules,

$$\alpha_2 \propto \alpha_1 \frac{C_2}{C_1} = \alpha_1 \frac{800\ ppm}{400\ ppm} = 2\alpha_1$$

so that in *State 2*,

$$k_2^{wings} = \frac{16\sigma}{3\left(2\alpha_1\right)} T_1^3 = 3{,}630 \frac{W}{m\ K}$$

$$q_2^{wings} \sim f^{wings} k_2^{wings} \frac{dT_1}{dz} = 2.794 \frac{W}{m^2}.$$

Radiative forcing from *State 1*, to *State 2* is:

$$\Delta q_{1-2}^{wings} = q_1^{wings} - q_2^{wings} = 2.794 \frac{W}{m^2}$$

4.2.3. Radiative forcing from C_1=400 ppm to C_3=4,000 ppm

In the hypothetical State 3, using $C_3 = 10\ C_1 = 4000\ ppm$ yields,

$$\alpha_3 \propto \alpha_1 \frac{C_3}{C_1} = \alpha_1 \frac{4000\ ppm}{400\ ppm} = 10\alpha_1$$

$$k_3^{wings} = \frac{16\sigma}{3\left(10\alpha_1\right)} T_1^3 = 726 \frac{W}{m\ K}$$

$$q_3^{wings} \sim f^{wings} k_3^{wings} \frac{dT_1}{dz} = 0.559 \frac{W}{m^2}.$$

Radiative forcing from *State 1*, to *State 3* is:

$$\Delta q_{1-3}^{wings} = q_1^{wings} - q_3^{wings} = 5.588 \frac{W}{m^2} - 0.559 \frac{W}{m^2} = 5.029 \frac{W}{m^2}.$$

4.3 The temperature increase ΔT caused by radiative forcing

For a small variation in temperature [34, 35], Stefan-Boltzmann's law, eq.(15), yields,

$$\Delta q = 4\sigma T^3 \Delta T = 4\sigma T^4 \frac{\Delta T}{T}$$

and,

$$\frac{\Delta q}{q} = 4\frac{\Delta T}{T}$$

so that ECS, i.e. the temperature increase ΔT, needed to compensate for reduced heat flux Δq is,

$$\Delta T = \frac{1}{4}\frac{\Delta q}{q} T \qquad (27)$$

Table 4 Radiative forcing *Δq* and *ΔT*

		Δq [Wm^{-2}] due to CO_2	ΔT [K] due to CO_2
State 0 (280 ppm) to State 1 (400 ppm)	The Wings Model α_1 =0.001[m^{-1}]; α_0 =0.0007[m^{-1}] The central PQR region is opaque	2.40	~0.58 using eq. (27)
	IPCC, 2013 [24,32] see Fig. 12	1.68 (1.50 to 1.86)	0.34 to 0.42 using eq. (27)
	Actual i.e. measured ΔT = 1.1 K, due to greenhouse gases, aerosols, land use etc.		1.1 measured
State 1 (400 ppm) to State 2 (800 ppm)	The Wings Model α_1 =0.001[m^{-1}]; α_2 =0.002[m^{-1}] The central PQR region is opaque	2.79	~0.67 using eq. (27)
	van Wijngaarden and Happer, see Fig.4 in [23]	3.0	0.72 using eq. (27)
	Harde [22]	3.77	1.09
	Harde [31]	2.4	0.6 to 0.8
State 1 (400 ppm) to State 3 (4000 ppm)	The Wings Model α_1 =0.001[m^{-1}]; α_3 =0.01[m^{-1}] The central PQR region is opaque	5.03	~1.2 using eq. (27)

5. Summary and Discussion

5.1 Measured absorbance of CO_2 at 295 K

The FTIR spectra in Figs 4-9 are comparable to the spectra constructed using the HITRAN database [3, 27-29]. The spectra shown in Fig 4 and 5, cover the same range and have higher resolution than the spectra available in the textbooks. There is no significant broadening due to increasing CO_2 pressure.

Table 1 contains the average values of $\boldsymbol{\alpha(\lambda)}$ in 2.70 μm, 4.26 μm and 15 μm bands, and range of pressure $0.04\ atm < p < 1\ atm$.

5.2 Measured α(λ) of air at 295 K

The spectral absorption coefficient $\boldsymbol{\alpha(\lambda)}$, for air containing 400 ppm of CO_2 and undetermined amount of H_2O, is given in Fig.10. Our spectrum are re-plotted as transmittance in Fig. 11, to enable comparison with the spectra constructed based on HITRAN database [29]. The shape and number of absorption peaks in the *P, Q* and *R* branches and the wings regions are virtually identical, see Fig. 11.

Table 2 holds the average values of $\boldsymbol{\alpha}$ for CO_2 in the *PQR* branches and in the wings region of the 15 μm band. $\boldsymbol{\alpha}$ in *2.7 μm* and *4.3 μm* bands of no interest because the fraction of radiation emitted by Earth is microscopic. Based on the FTIR spectra given in Fig. 10 b) and Fig. 11, at the present level of CO_2:

i) In the ***PQR branches***, the average value the absorption coefficient $\boldsymbol{\alpha = 0.085\ m^{-1}}$. With practically no lose in accuracy, the PQR part of the 15 μm band (13.8 μm to 16.3 μm) can be modeled as opaque.

ii) The wings region extends from 12.5 μm to 13.8 μm on the R-side and from 16.3 μm to 17 μm on the P-side. In the ***wings region***, $\alpha(\lambda)$ was hard to measure precisely, because of the low absorbance. $\boldsymbol{\alpha = \sim 0.001\ m^{-1}}$ given in Table 2, is the best estimate at present. More measurements are needed of the 15 μm band.

In short, only the wings region of the 15 μm band is active in radiative forcing.

5.3 The Wings region model

The number of parameters/components that could be influencing the climate is large, see Fig. 12. The potential interactions between the parameters further contribute to uncertainty of the predictions, so that the comprehensive line-by-line calculations, diverge by a factor of ~ 10. Considering the disagreement between the comprehensive models, focusing on CO_2 alone, seems practical.

In Table 4 radiative forcing calculated by the Wings model is compared to the data in the literature.

Considering the radiative forcing from the pre-industrial time to present (***280 ppm to 400 ppm***), the Wings

model estimates $\Delta q^{Wings}{}_{0\to1}$= 2.40 Wm^{-2}, see Table 4 a). The estimated temperature increase is ΔT = ~ 0.58 K. Both approximations are reasonable, considering that the IPCC report in 2013 gave the range of forcing $\Delta q^{IPCC}{}_{0\to1}$ =1.50 to 1.86 Wm^{-2} (see Fig. 12). Moreover, the actual measured ΔT (caused by all greenhouse gases including CO_2, aerosols, land use, etc.) from the pre-industrial time to present is 1.1 to 1.2 K.

Considering radiative forcing from ***400 ppm to 800 ppm***, the Wings-model yields $\Delta q^{Wings}{}_{1\to2}$~ 2.79 Wm^{-2}, see Table 4. This result is in a solid agreement with van Wijngaarden and Happer's the line by line calculations based on ~1/3 million HITRAN data-lines accounting for absorption by the five most abundant greenhouse gases, see Fig. 13 reproduced from [23]. The smooth blue line is the Planck's law. The area between the black line (*f=1*, 400 ppm) and red line (*f=2*, 800 ppm) is radiative forcing $\Delta q^{[23]}{}_{1\to2}$ = 3.0 Wm^{-2}, which is 6.9 % higher than the prediction by the Wings model. Additionally, the black and red lines ***overlap:***

a) in the center of the 15 μm band, confirming that the *PQR* ranches are saturated.

b) outside of the 15 μm band (i.e. in "windows"), confirming zero absorption by CO_2, molecules.

The black and red lines ***diverge*** at the edges of the 15 μm band, confirming that ***only the wings*** regions participate in radiative forcing.

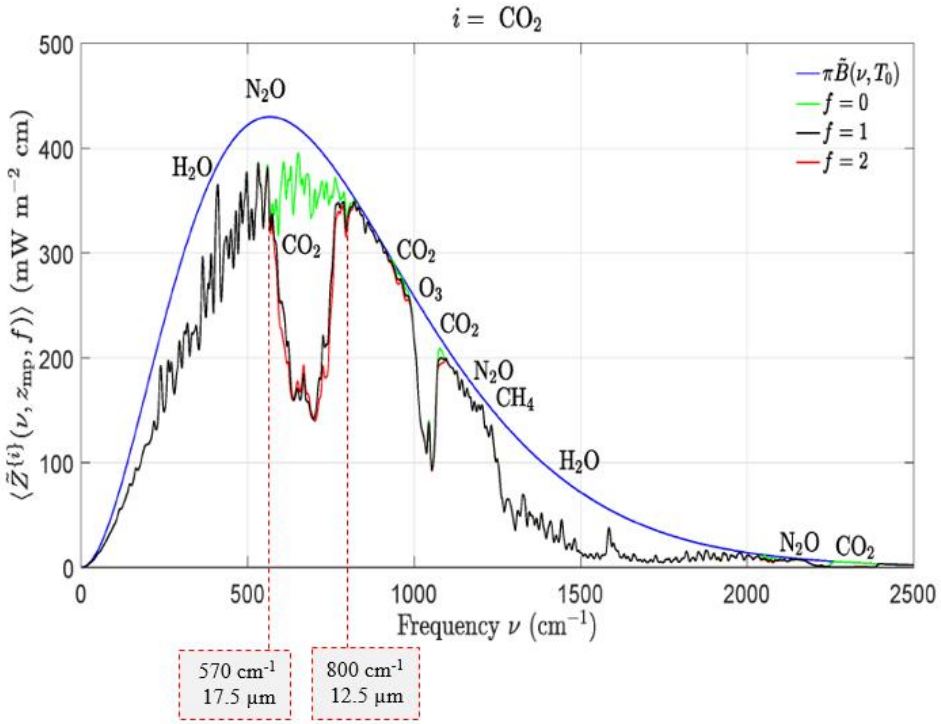

Fig. 13 Effects of changing CO_2 concentrations on transmitted spectral flux. The smooth blue line is the Planck's law. The green line (*f=0)* matches zero ppm. The black line (*f=1*) matches 400 ppm. The red line (*f=2*) matches 800 ppm. The area between *f=1* and *f=2* is Δq = 3.0 Wm^{-2}. Replicated from [23], with dashed lines showing 12.5 μm and 17.5 μm added.

6. Conclusions

1. The spectra presented in Figs. 10 and 11 a) and the comprehensive simulations based on the HITRAN database shown in Fig. 11b) and 13 demonstrate that ***CO_2 alone can cause radiative forcing only in the wings***

region of the 15 μm band.

2. The Wings model is a first order approximation. It predicts radiative forcing of $\Delta q_{1\to 2}$=2.79 Wm^{-2}, ~ 7 % lower value than the forcing reported in [23], see Table 4.

3. In the wings region, α_1= ~0.001 m^{-1} was calculated using eq. (27), from the preliminary spectral absorbance $\alpha_1(\lambda)$ given in Fig. 10 b). Using α_1 =0.00093 m^{-1} (~7% lower value) yields $\Delta q_{1\to 2}$ =3.0 Wm^{-2} which is equal to the forcing predicted by van Wijngaarden and Happer, see Fig. 13.

As a final note, at present, the thermal radiation flux transmitted through the ***wings region*** is q_1= 5.59 Wm^{-2}. The tenfold increase of CO_2 concentration to State 3 (assuming $\alpha_3 = 10\,\alpha_1$) yields a tenfold reduction in the heat flux, to q_3^{wings} =0.556 Wm^{-2}. Thus, a 10x increase in CO_2 concentration would result in 1.8x increase in radiative forcing, from $\Delta q_{1-2}{}^{wings}$ = 2.79 Wm^{-2} to $\Delta q_{1-3}{}^{wings}$ 5.03 Wm^{-2}. In short, at 4000 ppm, the wings region is close-to saturated, so that ΔT can not exceed ~ 1.5 K regardless of the CO_2 concentration.

To corroborate the above conclusions, more FTIR absorbance spectra are needed covering the 15 μm with 0.5 cm^{-1} resolution. To be reported in [26] along with line-by-line calculations [26].

References

[1] J.H. Lienhard "A Heat Transfer Textbook", Prentice-Hall, Inc. 1987.

[2] H.C. Hottel and A.F. Sarofim, "Radiative Transfer", McGraw-Hull Book Company (1967).

[3] Michael F. Modest, "Radiative Heat Transfer", Elsevier (2013) Third Edition.

[4] H.C. Hottel, "Radiation" Chapter IV of "Heat Transmission" by W.H. McAdams, McGraw-Hull Book Company (1954) 3rd Ed.

[5] B. Leckner "The Spectral and Total Emissivity of Water Vapor and Carbon Dioxide", Combustion and Flame 19 (1972) p33-48

[6] L.R. Glicksman, J.H. Lienhard V, Modeling and Approximation in Heat Transfer, Cambridge University Press, 2016.

[7] Edwards, D. K., Radiation Heat Transfer Notes", Hemisphere, Washington D.S. (1981).

[8] D.K. Edwards, Absorption by Infrared Bands of CO2 Gas at elevated Temperatures and Pressures." "Journal of the Optical Society of America, Vol. 50, Issue 6, pp. 617-626 (1960); https://doi.org/10.1364/JOSA.50.000617

[9] M. N. Ozisik, Basic Heat Transfer, McGraw-Hill Book Company, (1977)

[10] A. F. Milles, Heat Transfer", Irwin 1992

[11] W. Rohsenow and H.Y. Choi, "Heat Mass and Momentum Transfer", Prentice-Hall, Englewood Cliffs, NJ, 1961.

[12] R. Siegel and J.R. Howell (1981) "Thermal Radiation Heat Transfer", 2nd Ed. Hemisphere. 2nd Ed. McGraw-Hill NY 1981.

[13] Y.A. Cengel & A.J. Ghajar. "Heat and Mass Transfer Fundamentals & Applications". 4th ed. (2007) McGraw-Hill

[14] J. N. Howard, (1959)" The Transmission of the Atmosphere in the Infrared", 1452 PROCEEDINGS OF THE IRE

[15] Howard and Garing "The transmission of the atmosphere in the infrared" Infrared Physics. 1962, Vol. 2, pp. 155-173.

[16] J. H. Shaw, "The Ohio State University, Columbus, Ohio, Final Rept. Contract No. AF19(122)-65; 1954.

[17] Handbook of IR Military Technology (1965).

[18] Data from NIST Standard Reference Database 69: NIST Chemistry WebBook https://webbook.nist.gov/cgi/cbook.cgi?ID=C124389&Units=SI&Type=IR-SPEC&Index=1

[19] McClatchey, R. A., W. S. Benedict, S. A. Clough, D. E. Burch, K. Fox, L. S. Rothman, and J. S. Garing: "AFCRL atmospheric absorption line parameters compilation," Technical Report AFCRL-TR-0096, 1973.

[20] Rothman, L. S., R. R. Gamache, A. Goldman, L. R. Brown, R. A. Toth, H. M. Pickett, R. L. Poynter, J.-M. Flaud, C. Camy-Peyret, A. Barbe, N. Husson, C. P. Rinsland, and M. A. H. Smith: "The HITRAN database: 1986 edition," Applied Optics, vol. 26, no. 19, pp. 4058–4097, 1987.

[21] L. S. Rothman et al. "The HITRAN 2008 molecular spectroscopic database," Journal of Quantitative Spectroscopy and Radiative Transfer, vol. 110, pp. 533–572, 2009.

[22] H. Harde," Radiation Transfer Calculations and Assessment of Global Warming by CO_2", International Journal of Atmospheric Sciences Volume 2017, Article ID 9251034. https://doi.org/10.1155/2017/9251034

[23] W. A. van Wijngaarden and W. Happer, "Dependence of Earth Temperature on Five Most Abundant Greenhouse Gases", arXiv:2006.03098v1 [physics.ao-ph] 4 Jun 2020.

[24] Stocker, T.F., D. Qin, G.-K. Plattner, L.V. Alexander, S.K. Allen, N.L. Bindoff, F.-M. Bréon, J.A. Church, U. Cubasch,S. Emori, P. Forster, P. Friedlingstein, N. Gillett, J.M. Gregory, D.L. Hartmann, E. Jansen, B. Kirtman, R. Knutti, K.Krishna Kumar, P. Lemke, J. Marotzke, V. Masson-Delmotte, G.A. Meehl, I.I. Mokhov, S. Piao, V. Ramaswamy, D.Randall, M. Rhein, M. Rojas, C. Sabine, D. Shindell, L.D. Talley, D.G. Vaughan and S.-P. Xie, 2013: Technical Summary. In: Climate Change 2013: The Physical Science Basis. Contribution of Working Group I to the Fifth Assessment Report of the Intergovernmental Panel on Climate Change [Stocker, T.F., D. Qin, G.-K. Plattner, M. Tignor, S.K. Allen, J. Boschung, A. Nauels, Y. Xia, V. Bex and P.M. Midgley (eds.)]. Cambridge University Press, Cambridge, United Kingdom and New York, NY, USA.

[25] A.G. Ostrogorsky, Yao, A.F. Witt "Infrared Absorbance of B_20_3 at Temperature to 1250 C", Journal of Crystal Growth 84 (1987) 460—466.

[26] A.G. Ostrogorsky, "Absorbance and transmittance spectra of CO2 in air , in preparation." (2024).

[27] Modest, M. F., and S. P. Bharadwaj: "High-resolution, high-temperature transmissivity measurements and correlations for carbon dioxide–nitrogen mixtures," J. Quantitative Spectroscopy and Radiative Transfer, vol. 73, no. 2–5, pp. 329–338, 2002.

[28] M. F. Modest, S.P. Bharadwaj "Medium resolution transmission measurements of CO2 at high temperature", J. Quantitative Spectroscopy & Radiative Transfer 73 (2002) 329–338.

[29] H. Harde (2013) " Radiation and Heat Transfer in the Atmosphere: A Comprehensive Approach on a Molecular Basis", International J. Atmospheric Sciences, Vol. 2013, Article ID 503727, pp1-26 http://dx.doi.org/10.1155/2013/503727

[30] Peng-Sheng Wei∗, Yin-Chih Hsieh, Hsuan-Han Chiu, Da-Lun Yen, Chieh Lee, Yi-Cheng Tsai, Te-Chuan Ting, "Absorption coefficient of carbon dioxide across atmospheric troposphere layer, Heliyon 4 (2018) e00785.doi: 10.1016/j.heliyon.2018.e00785; https://doi.org/10.1016/j.heliyon.2018.e00785

[31] IPCC, 2013: Climate Change 2013: The Physical Science Basis. Contribution of Working Group I to the Fifth Assessment Report of the Intergovernmental Panel on Climate Change [Stocker, T.F., D. Qin, G.-K. Plattner, M. Tignor, S.K. Allen, J. Boschung, A. Nauels, Y. Xia, V. Bex and P.M. Midgley (eds.)]. Cambridge University Press, Cambridge, United Kingdom and New York, NY, USA, 1535 pp.

[32] C.L. Tien, "Thermal Radiation Properties of Gases", in Advances in Heat Transfer 5, Academic Press, New

York, pp. 253–324, 1968.

[33] C.L. Tien, “Flame Radiation”, Prog. Energy Combustion Sci. 8 (1982) pp44-5

[34] S. E. Schwartz, Resource Letter GECC-2: The Greenhouse Effect and Climate Change: The Intensified Greenhouse Effect”, Submitted to American Journal of Physics, 2018.

[35] S. E. Schwartz, Resource Letter GECC-1: The Greenhouse Effect and Climate Change: Earth's Natural Greenhouse E_ect, Am. J. Phys. 86, (8), 565-576, (2018).

NOMENCLATURE

A-absorbance
C – concentration, ppm.
Cs- Climate Sensitivity
ECS- Equilibrium Climate Sensitivity
FTIR- Fourier Transfer Infra-Red spectrometer
IPCC-Intergovernmental Panel on Climate Change
ath length, m
umber
pressure, atm or mmHg
= Radiative Forcing
mperature, K
T-transmittance

Greek symbols
α-absorption coefficient, m^{-1}
α(λ)- spectral absorption coefficient. m^{-1}
ν-Wave number, cm^{-1}
τ-transmittance.

Subscripts
0- State 0, C_0=280 ppm
1- State 1, C_1=400 ppm
2- State 2, C_1=800 ppm
3- State 3, C_1=4000 ppm

Submitted: 22.12.2024.
Revised: 14.1.2025.
Accepted: 27.1.2025.